Simulation and optimization of polymer-coated microsphere resonators in chemical vapor sensing

Nai Lin,[1] Lan Jiang,[1,*] Sumei Wang,[1] Qianghua Chen,[1] Hai Xiao,[2] Yongfeng Lu,[3] and Hailung Tsai[4]

[1]Laser Micro/Nano Fabrication Laboratory, School of Mechanical Engineering, Beijing Institute of Technology, Beijing 100081, China

[2]Department of Electrical and Computer Engineering, Missouri University of Science and Technology, Rolla, Missouri 65409, USA

[3]Department of Electrical Engineering, University of Nebraska–Lincoln, Lincoln, Nebraska 68588-0511, USA

[4]Department of Mechanical and Aerospace Engineering, Missouri University of Science and Technology, Rolla, Missouri 65409, USA

*Corresponding author: jianglan@bit.edu.cn

Received 9 May 2011; revised 6 July 2011; accepted 27 July 2011; posted 29 July 2011 (Doc. ID 147117); published 30 September 2011

This study presents a chemical vapor sensor based on polymer-coated microsphere resonators. A theoretical simulation of the sensor response is performed, and optimization of the polymer layer thickness is investigated. Results show that the sensor exhibits a good linearity and a low detection limit of the refractive index change. Especially at the thermostable thickness of the polymer layer, the refractive index detection limit of the wavelength around 780 nm can be as low as $\sim 2 \times 10^{-8}$ refractive index unit for a spectral resolution of 10 fm, without any temperature control. Because of the good sensing performance and simple manipulation, the proposed sensor is a very promising platform for chemical vapor detections.

OCIS codes: 140.4780, 230.5750, 280.4788, 160.5470.

1. Introduction

Optical microresonators of various shapes, such as microspheres [1–3], microdisks [4], and microtubes [5,6], have attracted a good deal of attention in sensing applications. In such resonators, the light propagates in the form of whispering gallery modes (WGMs) due to the total internal reflection of the light along the curved boundary between the high and low refractive index (RI) materials. Resonators with WGMs can achieve extremely high Q factors, and thus provide an effective long interaction length between the light and the analytes [7]. This would significantly reduce the amount of samples needed for detections, compared with conventional waveguide based sensors. For instance, a Q factor on the order of 10^9 has been reported for WGMs in fused-silica microspheres [8].

More recently, it has been discovered that the unique combination of optical microresonators and polymer materials could be used to develop highly sensitive optical chemical sensors [9–12]. As shown in Fig. 1, the optical microresonator is functionally coated with a thin layer of polymer. When interacting with vapor molecules, the polymer undergoes RI change and/or thickness change, which induces a resonant wavelength shift ($\delta\lambda_R$ in Fig. 1) in the transmission spectrum. Hence, by measuring the wavelength shift, it is possible to estimate the chemical

0003-6935/11/285465-08$15.00/0

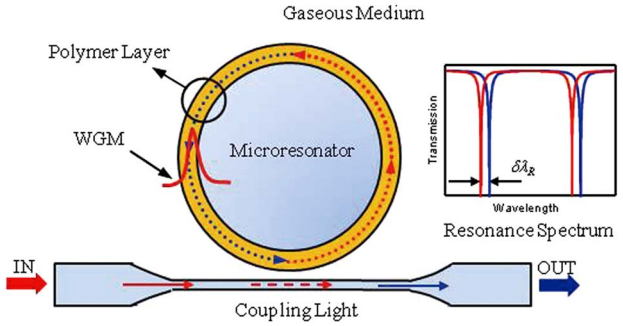

Fig. 1. (Color online) Polymer-coated microresonator chemical vapor sensor configuration.

vapor concentration in a gaseous medium surrounding the sensor. Such miniaturized sensors capable of *in situ* detection of chemical vapor have broad applications in many key areas, such as homeland security, environmental management, industrial process control, and public health. Passaro *et al.* propose a very compact optical ammonia sensor based on a silicon-on-insulator ring resonator coated with a layer of polymer [10]. But the sensitivity is relatively low [thus a large detection limit (DL)] because the WGMs are mainly confined to the vicinity of the resonator surface. Sun *et al.* develop a highly sensitive chemical vapor sensor based on a microtube resonator whose exterior or interior surface is coated with a polymer layer [11,12]. However, the fabrication of such a microtube sensor is rather difficult. In addition, the microtube is very brittle and thus difficult to handle in practical sensing application.

This study presents a chemical vapor sensor based on a polymer-coated microsphere resonator. The presented sensor utilizes the electric field confined within the polymer layer for chemical sensing, which is different than a conventional microsphere sensor where the evanescent field outside the sphere resonator is relied on for sensing. To the best of our knowledge, a free-standing microsphere whose surface is coated with a layer of polymer has not been explored for vapor sensing. Compared with the chemical sensors based on microring or microtube resonators, the microsphere sensors have larger Q factors and are easier to fabricate. Recent theoretical and experimental works on the polymer-coated WGM resonators [13–16] provide a basis for implementation of the proposed sensor. For the resonant RI sensors, both the RI sensitivity and DL must be presented to fully describe the sensor performance [17]. The numerical models to analyze the RI sensitivity and DL are demonstrated in Section 2. Based on the models, the sensing performance for the WGMs of different polarizations and orders are simulated in Section 3. Major results are reported in Section 4.

2. Theory

A. Sensing Principle

Over the years, the WGM modal structures and resonance spectra of microspheres have been widely studied [18–20]. WGM is characterized by a set of integers: l, m, and v, which represent angular, azimuthal, and radial mode numbers, respectively. For an ideal sphere, modes with the same l and v, but arbitrary m have the same resonant wavelength. Also, a WGM has either TE or TM polarization, and the two polarizations can be selectively excited by controlling the polarization of the coupling light. Considering a microsphere with the radius of a_0 coated by a polymer layer with the thickness of h_0, the characteristic equation to specify the resonant wavelengths λ_R of the WGMs can be expressed by [21,22]

$$N_0\frac{\chi_l'(k_0n_3a_1)}{\chi_l(k_0n_3a_1)}=\frac{B_l\psi_l'(k_0n_2a_1)+\chi_l'(k_0n_2a_1)}{B_l\psi_l(k_0n_2a_1)+\chi_l(k_0n_2a_1)},$$
$$N_0=\begin{cases}n_3/n_2, & \text{TE modes}\\ n_2/n_3, & \text{TM modes}\end{cases}, \tag{1}$$

where $k_0=2\pi/\lambda_R$ is the resonant wave vector; n_1, n_2 and n_3 are the RIs of the microsphere, the polymer layer and the surrounding medium, respectively; $a_1=a_0+h_0$ is the total radius of the whole microsphere including the polymer layer; ψ_l and χ_l are spherical Ricatti–Bessel function and spherical Ricatti–Neumann function, respectively; B_l is a coefficient and its expression is given by

$$B_l=\frac{N_1\psi_l'(k_0n_1a_0)\chi_l(k_0n_2a_0)-\psi_l(k_0n_1a_0)\chi_l'(k_0n_2a_0)}{\psi_l(k_0n_1a_0)\psi_l'(k_0n_2a_0)-N_1\psi_l'(k_0n_1a_0)\psi_l(k_0n_2a_0)},$$
$$N_1=\begin{cases}n_1/n_2, & \text{TE modes}\\ n_2/n_1, & \text{TM modes}\end{cases}. \tag{2}$$

For a given value of l, there are multiple values of λ_R that satisfy the characteristic equation. These resonant modes are called the first-order mode, the second-order mode…, and the vth order mode in the decreasing value of λ_R. According to the characteristic equation, when the polymer layer undergoes a RI change (δn_2) and/or a thickness change (δh_0), a shift $\delta\lambda_R$ in the resonant wavelength would take place correspondingly. For simplicity, this study considers the RI change only.

B. RI Sensitivity

For the TE and TM modes, the RI sensitivity (S) of the wavelength shift versus the surface layer RI change can be respectively given by [23]

$$S_{\text{TE}}=\frac{\lambda_R n_2 I_2}{\sum_{i=1}^{3}n_i^2 I_i}=\frac{\lambda_R}{n_2}\eta_2, \tag{3}$$

$$S_{\mathrm{TM}} = \frac{\lambda_R^2[n_1 n_3 k_0 I_2 - n_3 A_l^2 \psi_l(k_0 n_1 a_0)\psi_l'(k_0 n_1 a_0) + n_1 C_l^2 \chi_l(k_0 n_3 a_1)\chi_l'(k_0 n_3 a_1)]}{2\pi n_1 n_2 n_3 \sum_{i=1}^{3} I_i}$$
$$= \frac{\lambda_R}{n_2}\eta_2 - \frac{\lambda_R^2[n_3 A_l^2 \psi_l(k_0 n_1 a_0)\psi_l'(k_0 n_1 a_0) - n_1 C_l^2 \chi_l(k_0 n_3 a_1)\chi_l'(k_0 n_3 a_1)]}{2\pi n_1 n_2 n_3 \sum_{i=1}^{3} I_i}, \quad (4)$$

where

$$I_1 = \int_0^{a_0} [A_l \psi_l(k_0 n_1 r)]^2 \mathrm{d}_r,$$
$$I_3 = \int_{a_1}^{\infty} [C_l \chi_l(k_0 n_3 r)]^2 \mathrm{d}_r,$$
$$I_2 = \int_{a_0}^{a_1} [B_l \psi_l(k_0 n_2 r) + \chi_l(k_0 n_2 r)]^2 \mathrm{d}_r, \quad (5)$$

A_l and C_l are the coefficients determined by

$$A_l = \frac{B_l \psi_l(k_0 n_2 a_0) + \chi_l(k_0 n_2 a_0)}{\psi_l(k_0 n_1 a_0)},$$
$$C_l = \frac{B_l \psi_l(k_0 n_2 a_1) + \chi_l(k_0 n_2 a_1)}{\chi_l(k_0 n_3 a_1)}, \quad (6)$$

and η_1, η_2, and η_3 denote the fractions of light energy distributed in the microsphere, the polymer layer, and the surrounding medium, respectively, which are expressed by

$$\eta_i = \frac{n_i^2 I_i}{n_1^2 I_1 + n_2^2 I_2 + n_3^2 I_3} \text{(TE modes)},$$
$$\eta_i = \frac{I_i}{I_1 + I_2 + I_3} \text{(TM modes)}, \qquad i = 1, 2 \text{ and } 3. \quad (7)$$

The unit of RI sensitivity is nm/RIU.

C. RI Detection Limit

The RI DL, defined as the smallest detectable RI change of the polymer layer, is given by [17]

$$\mathrm{DL} = \frac{R}{S}, \quad (8)$$

where R is the sensor resolution. Considering the resolution as 3σ of the total sensor noise, R can be calculated by [17]

$$R = 3\sigma = 3\sqrt{\sigma_{\mathrm{spect}}^2 + \sigma_{\mathrm{ampl}}^2 + \sigma_{\mathrm{temp}}^2}, \quad (9)$$

where σ_{spect}, σ_{ampl}, and σ_{temp} are the standard deviations of the spectral noise, amplitude noise, and thermal noise, respectively. Spectral noise denotes the deviation in determining the position of the resonance, which is limited by the spectral resolution of the measurement setup (including the optical source and the detection device). Amplitude noise refers to the cumulative noise added to the spectrum profile, including thermal and shot noise in the photodetector, laser relative intensity noise, and quantization error. The standard deviation of the amplitude noise is given by [17]

$$\sigma_{\mathrm{ampl}} \approx \frac{\lambda_R}{4.5(\mathrm{SNR}^{0.25})} \times \frac{1}{Q}, \quad (10)$$

where SNR is the signal to noise ratio. The total Q factor can be divided into two parts, including the intrinsic Q factor (Q_{in}) and the extrinsic Q factor (Q_{ex}). The Q_{in} factor is related to the quality of the resonator itself, and the Q_{ex} factor describes the light coupling condition between the resonator and the coupling fiber. In this study, the resonator is assumed to be undercoupled (i.e., $Q_{\mathrm{ex}} \gg Q_{\mathrm{in}}$), and thus the total Q factor is limited by the Q_{in} factor. It is known that the Q_{in} factor is determined by the lumped loss of light in the resonator, which includes the tunneling loss (also known as radiation loss), the scattering loss from surface irregularities, and the material absorption loss of light. Tunneling loss is due to the curvature of the waveguiding boundaries in the direction of propagation, and it is very small for a microsphere of $a_0 > 15\,\mu$m [19]. Considering a large silica microsphere coated with a detect-free and smooth-surface polymer layer, the Q_{in} factor is mainly determined by the absorption loss of light in the resonator materials [14,16], which can be expressed as

$$\frac{1}{Q_{\mathrm{in}}} \approx \frac{1}{(Q_{\mathrm{abs}})_{\mathrm{silica}}} + \frac{1}{(Q_{\mathrm{abs}})_{\mathrm{polymer}}}, \quad (11)$$

where $1/(Q_{\mathrm{abs}})_{\mathrm{silica}}$ and $1/(Q_{\mathrm{abs}})_{\mathrm{polymer}}$ denote the material absorption loss of light in the silica microsphere and the polymer layer, respectively. The absorption limited Q factors are further calculated by $(Q_{\mathrm{abs}})_{\mathrm{silica}} = 2\pi n_1/(\lambda_R \alpha_1 \eta_1)$ and $(Q_{\mathrm{abs}})_{\mathrm{polymer}} = 2\pi n_2/(\lambda_R \alpha_2 \eta_2)$ [8], where α_1 and α_2 are the optical attenuation coefficients of silica and polymer respectively.

The WGM resonance is also susceptible to thermal fluctuations due to the environmental temperature variations and probe-induced energy absorptions. Especially for RI sensors with high Q factors, the temperature instability significantly impairs the DL. The standard deviation of the temperature-induced spectral fluctuation can be calculated by

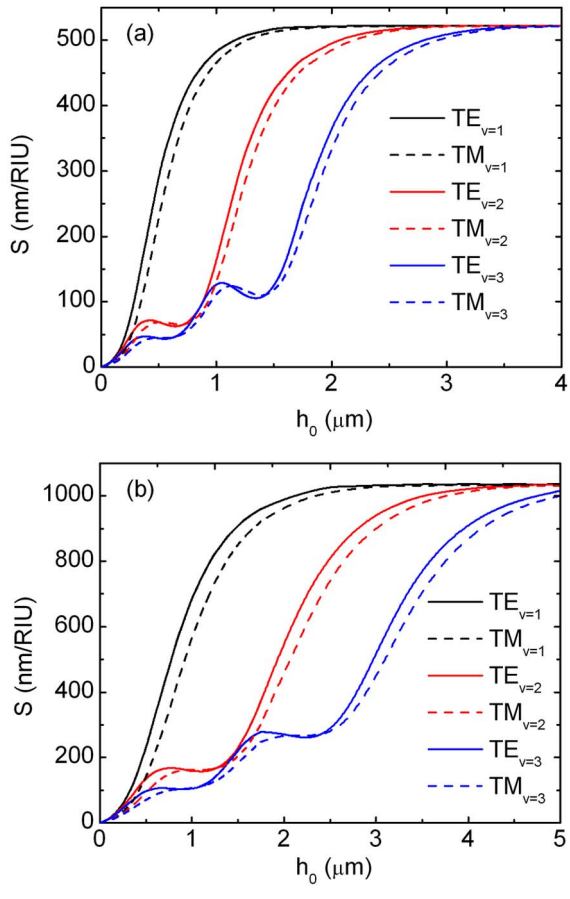

Fig. 2. (Color online) RI sensitivity S at the wavelength around (a) 780 nm and (b) 1550 nm, for TE modes (solid curves) and TM modes (dashed curves) of the first three orders as a function of the polymer layer thickness h_0.

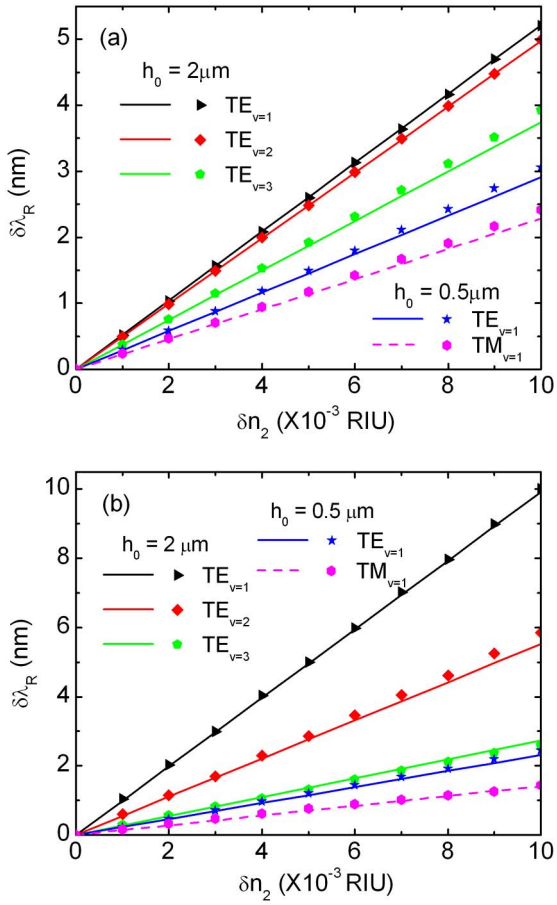

Fig. 3. (Color online) Resonance shift $\delta\lambda_R$ at the wavelength around (a) 780 nm and (b) 1550 nm as a function of the polymer layer RI change δn_2. The curves represent $\delta\lambda_R = S \times \delta n_2$. The symbols represent $\delta\lambda_R$ calculated by Eq. (1).

$$\sigma_{\text{temp}} \approx \lambda_R \left(\frac{1}{n_{\text{eff}}} \frac{dn_{\text{eff}}}{dT} + \frac{1}{a_1} \frac{da_1}{dT} \right) \sigma_T, \tag{12}$$

where σ_T is the standard deviation of the temperature variation; n_{eff} is the effective RI of the WGMs, which can be approximately expressed as $n_{\text{eff}} = \eta_1 n_1 + \eta_2 n_2 + \eta_3 n_3$. So, σ_{temp} is further expressed as

$$\sigma_{\text{temp}} \approx \lambda_R \left(\frac{\sum_{i=1}^{3} \eta_i (dn_i/dT)}{\sum_{i=1}^{3} (\eta_i n_i)} + \frac{\kappa_1 a_0 + \kappa_2 h_0}{a_0 + h_0} \right) \sigma_T, \tag{13}$$

where dn_1/dT, dn_2/dT, and dn_3/dT are the thermal refraction coefficients of the microsphere, the polymer layer, and the surrounding medium, respectively; κ_1 and κ_2 are the linear thermal expansion coefficients of the microsphere and the polymer layer. Substituting (7) into (13), σ_{temp} for TE and TM modes in the polymer-coated microsphere can be respectively given by

$$(\sigma_{\text{temp}})_{\text{TE}} \approx \lambda_R \left(\frac{\sum_{i=1}^{3} I_i n_i^2 (dn_i/dT)}{\sum_{i=1}^{3} (I_i n_i^3)} + \frac{\kappa_1 a_0 + \kappa_2 h_0}{a_0 + h_0} \right) \sigma_T, \tag{14}$$

$$(\sigma_{\text{temp}})_{\text{TM}} \approx \lambda_R \left(\frac{\sum_{i=1}^{3} I_i (dn_i/dT)}{\sum_{i=1}^{3} (I_i n_i)} + \frac{\kappa_1 a_0 + \kappa_2 h_0}{a_0 + h_0} \right) \sigma_T. \tag{15}$$

3. Simulation and Optimization of the Sensor

As an example, we consider a fused-silica microsphere of $a_0 = 50\,\mu$m coated with a polymer layer. The material of the polymer layer is selected to be polymethylmethacrylate (PMMA) doped with bromocresol purple (BCP). When exposed to ammonia, PMMA-BCP changes its RI at a wavelength beyond the absorption band (from 350 nm to 450 nm). For instance, ammonia diluted with pure nitrogen to a molar concentration of 5% could induce a RI change about 10^{-3} RIU of PMMA-BCP [24]. The polymer-coated resonator is assumed to be immersed in nitrogen, and coupled to a laser operating at $\lambda_R \approx 780$ and 1550 nm, respectively. The values of the RIs are chosen as $n_1 = 1.45$ for the fused-silica microsphere, $n_2 = 1.49$ for the PMMA layer, and $n_3 = 1.0$ for the nitrogen surrounding the PMMA-coated microsphere. Figure 2 shows the RI sensitivity as a function of the polymer layer thickness for both TE and TM modes of the first three orders. When the

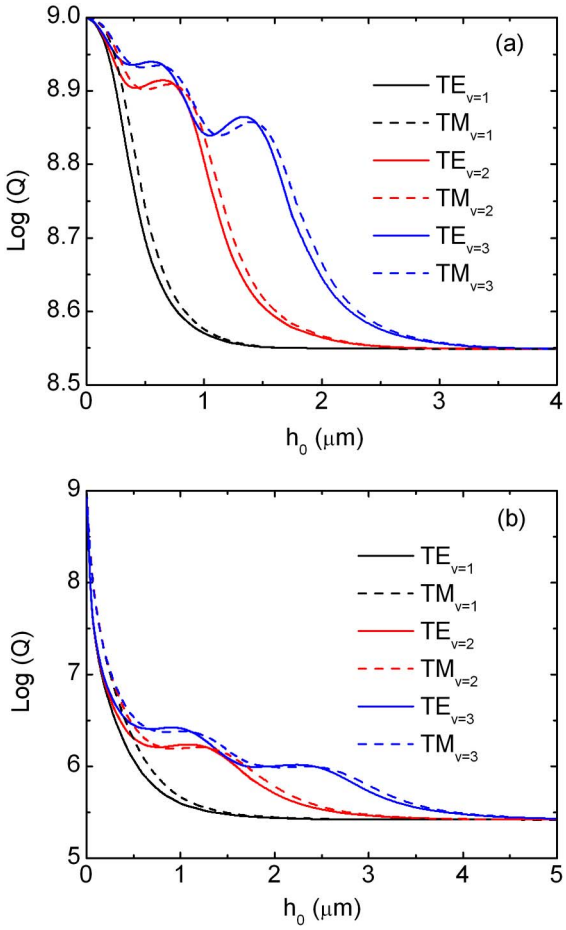

Fig. 4. (Color online) Q factor at the wavelength around (a) 780 nm and (b) 1550 nm as a function of the polymer layer thickness h_0.

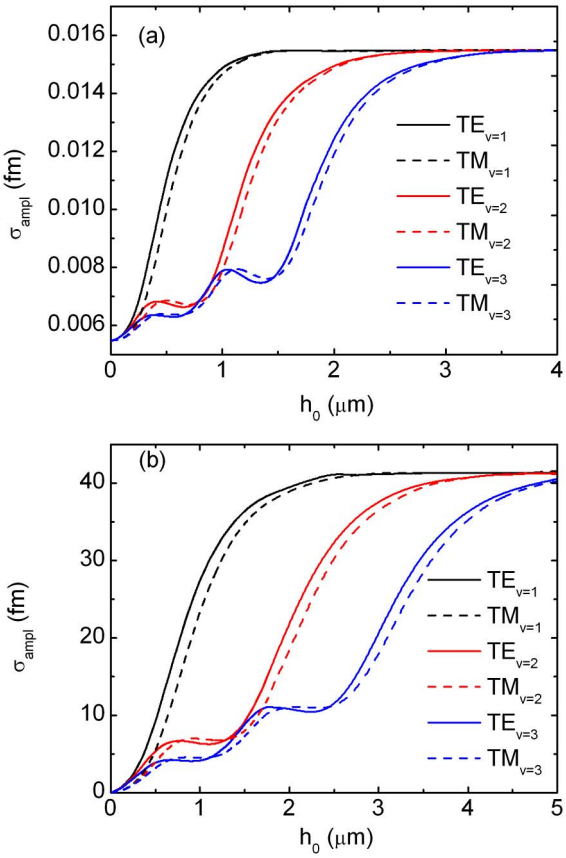

Fig. 5. (Color online) Amplitude noise standard deviation σ_{ampl} at the wavelength around (a) 780 nm and (b) 1550 nm as a function of the polymer layer thickness h_0, for a SNR of 60 dB.

polymer layer thickness increases, the RI sensitivity increases until it reaches the maximum, at which point the light energy in the silica microsphere is completely transferred into the polymer layer (i.e., $\eta_1 = 0$). And, the highest RI sensitivity is almost identical for all modes. But the WGM of a higher order needs a thicker polymer layer to achieve the highest RI sensitivity. According to (3) and (4), the RI sensitivity also increases with the detection wavelength. As shown by Fig. 2, the highest RI sensitivities are 522 and 1037 nm/RIU at $\lambda_R \approx 780$ and 1550 nm, respectively. Figure 3 plots the resonant wavelength shift as a function of the polymer layer RI change at $h_0 = 0.5$ and 2 μm. The curves represent the approximate results evaluated by $\delta\lambda_R = S \times \delta n_2$. The symbols denote the accurate results that are numerically calculated by substituting δn_2 into the resonance condition, Eq. (1). It is shown that the polymer-coated microsphere based RI sensors exhibit a good linear sensing characteristic in the range of RI changes, and the curves agree well with the accurate values.

When the polymer layer thickness increases, more light energy is distributed in the polymer (thus η_2 increases), which finally leads to a larger RI sensitivity. But, as η_2 increases, the Q factor is decreased due to the larger material absorption loss in polymer than silica. Especially at $\lambda_R \approx 1550$ nm, the optical attenuation coefficient α_2 of the polymer is ultrahigh, about 1 dB/cm (i.e., 23 m^{-1}) [25]. At $\lambda_R \approx 780$ nm, α_2 is about 0.15 dB/m (i.e., 0.03 m^{-1}). Figure 4 shows the Q factor as a function of the polymer layer thickness for both TE and TM modes of the first three orders. The Q factor of the silica microsphere before the polymer coating is taken to be 10^9 [16]. When η_2 increases with the layer thickness to have $\alpha_2\eta_2 \gg \alpha_1\eta_1$, the total Q factor is mainly determined by the large absorption loss in the polymer and thus can be approximated by $Q = 2\pi n/(\lambda_R\alpha_2\eta_2)$, which are 3.5×10^8 and 2.5×10^5 at $\lambda_R \approx 780$ and 1550 nm, respectively. Figure 5 shows σ_{ampl} for the RI sensor with a SNR of 60 dB, as a function of the polymer layer thickness. The amplitude noise is very low ($\sigma_{\text{ampl}} <$ 0.016 fm) at $\lambda_R \approx 780$ nm, due to the high Q factors. On the contrary, σ_{ampl} increases significantly with the polymer layer thickness at $\lambda_R \approx 1550$ nm, which is larger than 40 fm for a thick layer.

Figure 6 shows σ_{temp} as a function of h_0 for a temperature fluctuation of $\sigma_T = 10^{-3}$ K. At room temperatures, the linear thermal expansion coefficients of silica and PMMA-BCP are $\kappa_1 = 5.5 \times 10^{-7}$/K and $\kappa_2 = 5.0 \times 10^{-5}$/K, and the thermal refraction

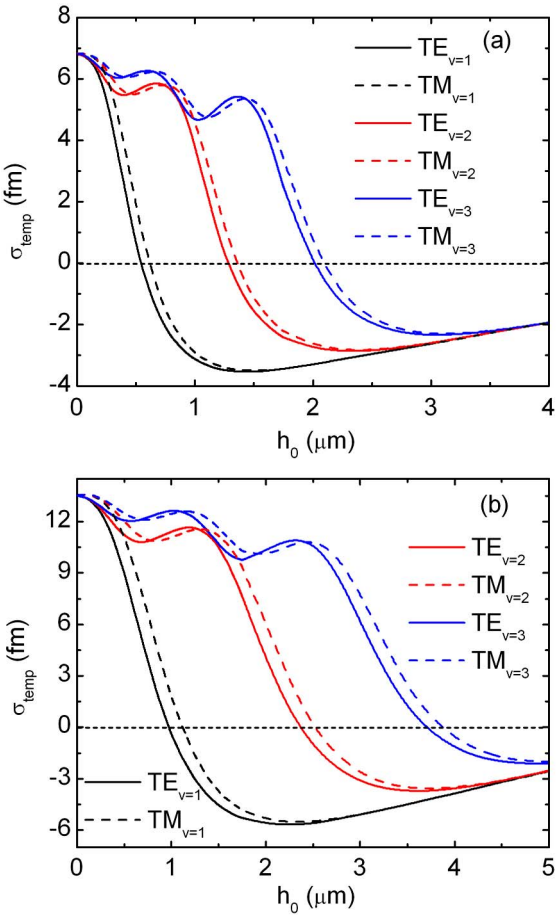

Fig. 6. (Color online) Thermal noise standard deviation σ_{temp} at the wavelength around (a) 780 nm and (b) 1550 nm as a function of the polymer layer thickness h_0, for a temperature fluctuation of $\sigma_T = 10^{-3}$ K.

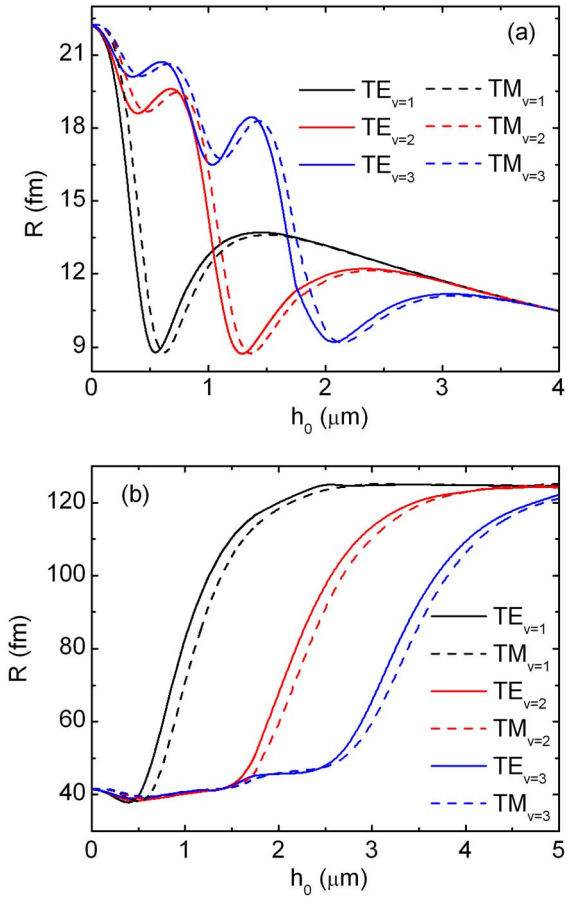

Fig. 7. (Color online) Sensor resolution R at the wavelength around (a) 780 nm and (b) 1550 nm as a function of the polymer layer thickness h_0, for SNR = 60 dB, $\sigma_{\text{spect}} = 2.9$ fm, and $\sigma_T = 10^{-3}$ K.

coefficients of silica and PMMA-BCP are $dn_1/dT = 1.19 \times 10^{-5}$/K and $dn_2/dT = -1.0 \times 10^{-5}$/K, respectively [14,24]. The negative sign of σ_{temp} denotes that the resonant wavelength decreases with the temperature increase. As the layer thickness increases, the negative thermal refraction of the polymer layer becomes dominant, which finally leads to the change of σ_{temp} from positive to negative. At $\lambda_R \approx 780$ nm, a near-zero thermal noise can be achieved at $h_0 \approx 0.6$, 1.3, and 2.0 μm, for the TE mode of the first, second, and third order, respectively. In the following discussion, the polymer layer thickness at which the thermal noise is near zero is referred as the thermostable thickness. Figure 6 shows that the thermostable thickness of the TM mode is slightly larger than that of the TE mode of the same order. Also, the thermostable thickness increases with the wavelength of the detection laser. For example, the thermostable thickness of the first-order TE mode is about 1.0 μm at $\lambda_R \approx 1550$ nm, which is larger than that at $\lambda_R \approx 780$ nm ($h_0 \approx 0.6\,\mu$m).

Because of the very narrow resonance linewidth of the WGM based RI sensors, a photodetector is usually used as the detection device to monitor the output signal, and the spectral resolution is mainly limited by the laser linewidth of the optical source, which is typically less than 1 MHz [17]. At the wavelengths around 780 and 1550 nm, 1 MHz is equivalent to about 2 and 8 fm, respectively. As a result, the spectral resolution can conservatively be assumed to be 10 fm in this study, which corresponds to a standard deviation of $\sigma_{\text{spect}} = 2.9$ fm. The theoretical predication of the Q factor at $\lambda_R \approx 780$ nm is higher than 3×10^8 (i.e., the resonance linewidth is smaller than 2.6 fm) as mentioned in Fig. 4(a), while the Q factor is about 10^8 in practice for the measurement setup with a spectral resolution of 10 fm. But, for a Q factor around 10^8, the amplitude noise is still very small ($\sigma_{\text{spect}} = \sim 0.07$ fm) as compared with the spectral noise. In addition, the sensor system is considered to be placed on a thermoelectric cooling unit, through which a temperature fluctuation of $\sigma_T = 10^{-3}$ K can be achieved [26]. Figure 7 plots the sensor resolution as a function of the polymer layer thickness, assuming the sensor with a SNR of 60 dB, a spectral noise of $\sigma_{\text{spect}} = 2.9$ fm, and a temperature fluctuation of $\sigma_T = 10^{-3}$ K. At $\lambda_R \approx 780$ nm, the amplitude noise is very small, and the lowest sensor resolution is about 9 fm at the thermostable thickness, which is limited by the spectral noise only. For a layer thickness

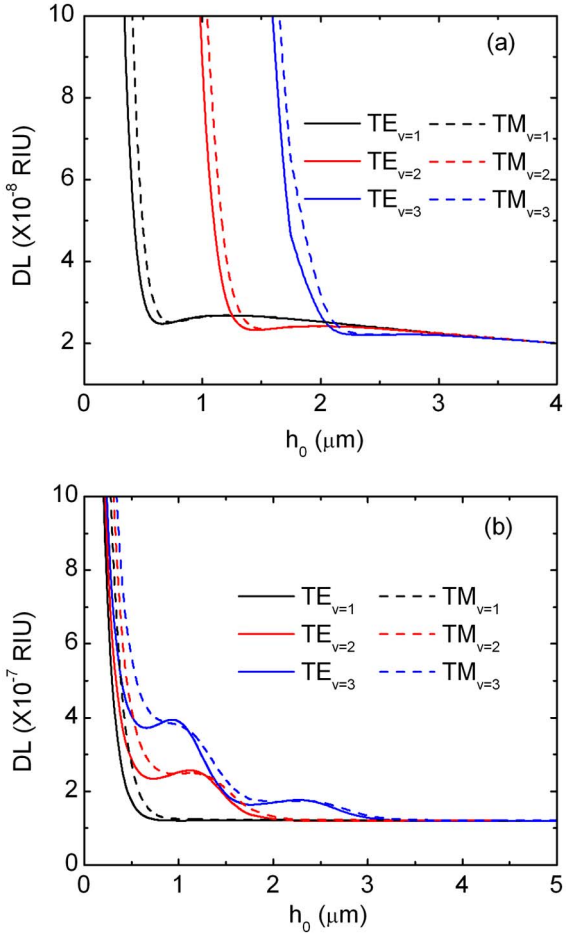

Fig. 8. (Color online) RI DL at the wavelength around (a) 780 nm and (b) 1550 nm as a function of the polymer layer thickness h_0, for SNR = 60 dB, $\sigma_{\text{spect}} = 2.9$ fm and $\sigma_T = 10^{-3}$ K.

beyond the thermostable thickness, the resolution is limited by both the spectral noise and the thermal noise. At $\lambda_R \approx 1550$ nm, due to the large amplitude noise, the resolution is much larger than that at $\lambda_R \approx 780$ nm. As a result, the WGM resonance around 780 nm might have a lower RI DL than that around 1550 nm, as shown in Fig. 8. With the layer thickness increases, the RI DL decreases quickly to about 2×10^{-8} RIU at $\lambda_R \approx 780$ nm, which corresponds to a minimum detectable ammonia concentration change of ~1 ppm. For a sensor system with a higher spectral resolution, the RI DL can be even smaller. For example, for a spectral noise of $\sigma_{\text{spect}} = 0.29$ fm, the RI DL of the WGM resonance around 780 nm is $\sim 2 \times 10^{-9}$ RIU (ammonia concentration change of ~0.1 ppm) at the thermostable layer thickness. The lowest DL at $\lambda_R \approx 1550$ nm is about 1×10^{-7} RIU, nearly one order larger than that at $\lambda_R \approx 780$ nm.

Figure 9 shows the RI DL changes with the layer thickness at different values of σ_T. It is shown that, for a layer thickness beyond the thermostable thickness, the RI DL is very susceptible to the temperature fluctuation. For instance, at $h_0 = 1\,\mu$m, the RI DL of the first-order TE mode around 780 nm is $\sim 2 \times 10^{-7}$ RIU at $\sigma_T = 10^{-2}$ K, which is about one

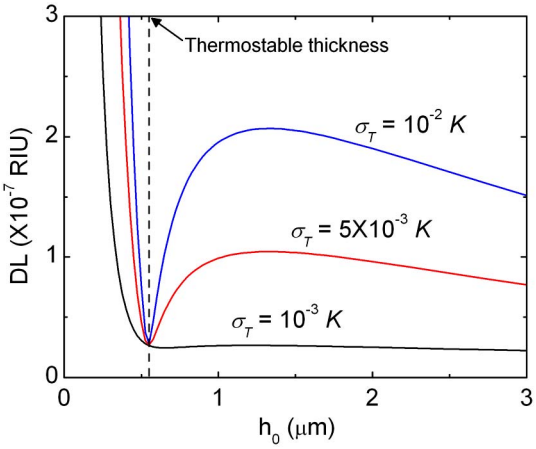

Fig. 9. (Color online) RI DL of the TE$_{v=1}$ mode around 780 nm as a function of the polymer layer thickness h_0, at $\sigma_T = 10^{-3}$, 5×10^{-3}, and 10^{-2} K respectively.

order larger than that at $\sigma_T = 10^{-3}$ K. However, at the thermostable thickness, the thermal noise is still near zero and thus the RI DL remains very small. So, for a large temperature fluctuation, the layer thickness should be optimized to be around the thermostable thickness to eliminate the resonance thermal response. Otherwise, better temperature control devices, such as thermoelectric cooling units, must be implemented to ensure a small temperature variation. The aforementioned analysis shows that the optimal thickness of the polymer layer (i.e., the thermostable thickness) is larger for the WGM of a higher order. But, for a thicker polymer layer, it takes a longer time for the vapor molecules to diffuse throughout the entire polymer layer and reach the equilibrium state, which corresponds to a longer response time of the chemical sensor. So, in practical applications of the polymer-coated microresonator based chemical sensor, the WGMs of a lower order should be selectively excited for a thinner optimal polymer layer and thus a shorter response time.

4. Conclusions

This study presents a chemical vapor sensor consisting of a microsphere resonator coated with a polymer layer. The dependence of the sensor performance on the polymer layer thickness is simulated for the WGMs of various orders and polarizations. The results show that, with the polymer layer thickness increases, more light energy is distributed in the polymer and thus leads to a higher RI sensitivity but a smaller Q factor (i.e., a larger amplitude noise). Especially at the wavelength around 1550 nm, the increase of the amplitude noise with the layer thickness is evident due to the significantly decreased Q factor. A further analysis shows that a near-zero thermal noise can be achieved at specific layer thicknesses (referred to as thermostable thicknesses), which increase with the WGM orders and the detection wavelength. At the thermostable thickness, the RI DLs of the WGM resonances around 780 and 1500 nm are as low as $\sim 2 \times 10^{-8}$ and $\sim 1 \times 10^{-7}$ RIU,

even if a large temperature fluctuation is induced to the sensor system.

This research is supported by the National Natural Science Foundation of China (NSFC) grants 90 923 039, 51 025 521, and 51 005 022).

References

1. F. Vollmer, D. Braun, A. Libchaber, M. Khoshsima, I. Teraoka, and S. Arnold, "Protein detection by optical shift of a resonant microcavity," Appl. Phys. Lett. **80**, 4057–4059 (2002).
2. S. Arnold, M. Khoshsima, I. Teraoka, S. Holler, and F. Vollmer, "Shift of whispering-gallery modes in microspheres by protein adsorption," Opt. Lett. **28**, 272–274 (2003).
3. N. M. Hanumegowda, C. J. Stica, B. C. Patel, I. M. White, and X. Fan, "Refractometric sensors based on microsphere resonators," Appl. Phys. Lett. **87**, 201107 (2005).
4. W. Fang, D. B. Buchholz, R. C. Bailey, J. T. Hupp, R. P. H. Chang, and H. Cao, "Detection of chemical species using ultraviolet microdisk lasers," Appl. Phys. Lett. **85**, 3666–3668 (2004).
5. T. Ling and L. J. Guo, "A unique resonance mode observed in a prism-coupled micro-tube resonator sensor with superior index sensitivity," Opt. Express **15**, 17424–17432 (2007).
6. I. M. White, H. Oveys, and X. Fan, "Liquid-core optical ring-resonator sensors," Opt. Lett. **31**, 1319–1321 (2006).
7. L. J. Guo and T. Ling, "Analysis of the sensing properties of silica microtube resonator sensors," J. Opt. Soc. Am. B **26**, 471–477 (2009).
8. M. L. Corodetsky, A. A. Savchenkov, and V. S. Ilchenko, "Ultimate *Q* of optical microsphere resonators," Opt. Lett. **21**, 453–455 (1996).
9. A. Ksendzov, M. L. Homer, and A. M. Manfreda, "Integrated optics ring-resonator chemical sensor with polymer transduction layer," Electron. Lett. **40**, 63–65 (2004).
10. V. M. N. Passaro, F. Dell'Olio, and F. De Leonardis, "Ammonia optical sensing by microring resonators," Sensors **7**, 2741–2749 (2007).
11. Y. Sun, S. I. Shopova, G. F. Mason, and X. Fan, "Rapid chemical-vapor sensing using optofluidic ring resonators," Opt. Lett. **33**, 788–790 (2008).
12. Y. Sun and X. Fan, "Analysis of ring resonators for chemical vapor sensor development," Opt. Express **16**, 10254–10267 (2008).
13. M. Han and A. Wang, "Temperature compensation of optical microresonators using a surface layer with negative thermo-optic coefficient," Opt. Lett. **32**, 1800–1802 (2007).
14. L. He, Y. F. Xiao, C. Dong, J. Zhu, V. Gaddam, and L. Yang, "Compensation of thermal refraction effect in high-*Q* toroidal microresonator by polydimethylsiloxane coating," Appl. Phys. Lett. **93**, 201102 (2008).
15. B. B. Li, Q. Y. Wang, Y. F. Xiao, X. F. Jiang, Y. Li, L. X. Xiao, and Q. H. Cong, "On chip, high-sensitivity thermal sensor based on high-*Q* polydimethylsiloxane-coated microresonator," Appl. Phys. Lett. **96**, 251109 (2010).
16. C. H. Dong, F. W. Sun, C. L. Zou, X. F. Ren, G. C. Guo, and Z. F. Han, "High-*Q* silica microsphere by poly(methyl methacrylate) coating and modifying," Appl. Phys. Lett. **96**, 061106 (2010).
17. I. M. White and X. D. Fan, "On the performance quantification of resonant refractive index sensors," Opt. Express **16**, 1020–1028 (2008).
18. R. L. Hightower and C. B. Richardson, "Resonant Mie scattering from a layered sphere," Appl. Opt. **27**, 4850–4855 (1988).
19. B. E. Little, J. P. Laine, and H. A. Haus, "Analytic theory of coupling from tapered fibers and half-blocks into microsphere resonators," J. Lightwave Technol. **17**, 704–715 (1999).
20. A. B. Matsko and V. S. Ilchenko, "Optical resonators with whispering-gallery modes—Part I: Basics," IEEE J. Quantum Electron. **12**, 3–14 (2006).
21. I. Teraoka and S. Arnold, "Enhancing the sensitivity of a whispering-gallery mode microsphere sensor by a high-refractive-index surface layer," J. Opt. Soc. Am. B **23**, 1434–1442 (2006).
22. I. Teraoka and S. Arnold, "Whispering-gallery modes in a microsphere coated with a high-refractive index layer: polarization-dependent sensitivity enhancement of the resonance-shift sensor and TE-TM resonance matching," J. Opt. Soc. Am. B **24**, 653–659 (2007).
23. N. Lin, L. Jiang, S. M. Wang, L. Yuan, H. Xiao, Y. F. Lu, and H. L. Tsai, "Ultrasensitive chemical sensors based on whispering gallery modes in a microsphere coated with zeolite," Appl. Opt. **49**, 6463–6471 (2010).
24. S. S. Sarkisov, D. E. Diggs, G. Adamovsky, and M. J. Curley, "Single-arm double-mode double-order planar waveguide interfereometric sensor," Appl. Opt. **40**, 349–359 (2001).
25. J. R. Schwesyg, T. Beckmann, A. S. Zimmermann, K. Buse, and D. Haertle, "Fabrication and characterization of whispering gallery mode resonators made of polymer," Opt. Express **17**, 2573–2578 (2009).
26. X. Fan, I. M. White, H. Zhu, J. D. Suter, and H. Oveys, "Overview of novel integrated optical ring resonator bio/chemical sensors," Proc. SPIE **6452**, 64520M (2007).